Korean J. Chem. Eng., 39(2), 431-439 (2022)
DOI: 10.1007/s11814-021-0905-2

pISSN: 0256-1115
eISSN: 1975-7220

Carbon coated MFe_2O_4 (M=Fe, Co, Ni) magnetite nanoparticles: A smart adsorbent for direct yellow and moderacid red dyes

Hoang Vinh Tran*,†, Hai Van Nguyen, Doanh Viet Vu**,***, Thu Dieu Le*, Binh Thanh Nguyen****, and Dang Hai Le**,†**

*School of Chemical Engineering, Hanoi University of Science and Technology (HUST), 1st Dai Co Viet Road, Hai Ba Trung District, Hanoi, Vietnam
**Faculty of Chemistry, Hanoi National University of Education (HNUE), 136 Xuan Thuy Road, Cau Giay District, Hanoi, Vietnam
***Faculty of Pharmacy, Hanoi University of Business and Technology (HUBT), 124 Vinh Tuy Street, Hai Ba Trung District, Hanoi, Vietnam
****Institute of Physics, Vietnam Academy of Science and Technology (VAST), 18 Hoang Quoc Viet Road, Cau Giay District, Hanoi, Vietnam
(*Received 23 May 2021 • Revised 6 July 2021 • Accepted 12 July 2021*)

Abstract−We report here a simple approach for synthesis of carbon coated magnetite (C@MFe_2O_4, M=Co, Ni, Fe) with shell@core nanostructured composites that we used as magnetic-nanosorbents for direct yellow (DYG) and moderacid red (RS) as pollutant textile dyes removal via an adsorption process. The synthesized C@MFe_2O_4 was characterized by TEM, SEM, EDX, XRD, FT-IR and VSM techniques. TEM results indicated that C@MFe_2O_4 nanocomposites have 20-30 nm of MFe_2O_4 nanoparticle core and 2-3 nm in thickness of the amorphous carbon shell. The synthesized C@MFe_2O_4 nanocomposites have the zero point charge (pH_{ZPC}) at 5.5, which suggests that DYG and RS, anionic dyes can be adsorbed onto the C@MFe_2O_4 nanosorbents in the acidic medium. Adsorption of DYG and RS onto magnetic nanosorbents was optimized and adsorption thermodynamic parameters were evaluated, clearly indicating that the adsorption of RS onto synthesized magnetic-nanosorbents was facile more than that DYG. The adsorption isotherm data showed that the adsorption processes of DYG and RS onto Fe_3O_4 or C@MFe_2O_4 nanosorbents are more suitable for the Langmuir model than Freundlich model. The maximum adsorption capacity (q_{max}) of DYG dye onto Fe_3O_4, C@Fe_3O_4 and C@$CoFe_2O_4$ adsorbents was 14.641, 36.232 and 7.85 mg g^{-1}, respectively; meanwhile, these values were 41.152, 61.728 and 39.683 mg g^{-1} for RS dye. These obtained data indicate that the developed Fe_3O_4, C@Fe_3O_4 and C@$CoFe_2O_4$ nanoparticles can be used as recoverable and recyclable adsorbents for not only organic pigments adsorption but also for heavy metal ion removal or protein extraction as well.

Keywords: Carbon Coated Magnetite, Core/Shell Structure Nanocomposites, Direct Yellow (DYG), Moderacid Red (RS), Organic Dyes, Adsorption

INTRODUCTION

Organic dyes present in wastewater, which are released from the dyeing and textile industries, are toxic, carcinogenic, resistant to aerobic digestion, and stable to oxidizing agents [1-10]. Although various treatment techniques have been reported, however, adsorption is still considered as one of the most economical and applicable methods to remove textile organic pollutants from wastewater. In fact, traditional adsorbents, such as chitosan above or including charcoal, activated carbon [11-13], clay [14,15], laterite, sand, silica [16-18], bentonite, montmorillonite, zeolites [19-21] or bio-sorbents, which are made from crop wastes [22-29] or plant wastes [30,31], can be used for water purification. However, they still have several limitations during applications, mainly for low adsorption capacity and the difficulty in recovering to regenerate. Therefore, it is a challenge and urgent need to develop new kinds of adsorbents with high adsorption capacity, good chemical stability; moreover, these adsorbents must be recoverable and recyclable for polluted water treatments via adsorption processes. To solve above inconveniences, magnetic separation technologies are operated based on the use of magnetic adsorbents. These techniques have received high attention for polluted organic dye treatment by the adsorption process due to its convenience, low-cost and efficient treatment. The magnetite nanoparticles containing-based adsorbents can be recovered after adsorption processes by applying an external magnetic field; thereby, they are recoverable and recyclable adsorbents.

In this work, we propose new magentite-based nanosorbents, which are prepared by coating an amorphous carbon layer onto various magnetite nanoparticles (C@MFe_2O_4 with M=Fe, Co, and Ni). The analyzed data indicated that the magnetite of F_3O_4 or $CoFe_2O_4$ or $NiFe_2O_4$ nanoparticles core was coated of a carbon layer, which supports a porous layer for enhancing adsorption capacity of the magnetic nanoparticles. In a synergistic activity, the presence of the

†To whom correspondence should be addressed.
E-mail: hoang.tranvinh@hust.edu.vn, danglh@hnue.edu.vn

magnetite nanoparticles is accepted, making a magnetic adsorbent, which can be simply recovered after adsorption process via magnetic field assisted separation technologies, for further regeneration and reuse. In the application part, we tested these adsorbents for adsorption of direct yellow GX (DYG) and moderacid red (RS) dyes. Herein, direct yellow GX [1,3,5] (a chrysophenine, $C_{30}H_{26}N_4Na_2O_8S_2$, M_w=680.66 g mol^{-1}) is named as DYG, which is a typical direct dye for yellow color in the textile. The (4E) -3- oxo- 4- [(4sulfonatonaphthalen-1 myl) hydrazinylidene] naphthalene -2,7-disulfonate (Moderacid Red (RS), ($C_{20}H_{11}N_2Na_3O_{10}S_3$, Amaranth (E123), M_w=604.48 g mol^{-1}) is a naphthylazo dye, which has been used for food colorization [32-34].

EXPERIMENTAL

1. Materials and Reagents

Iron (III) chloride hexahydrate ($FeCl_3{\cdot}6H_2O$, ≥98 wt%), ammonium iron (II) sulfate hexahydrate ($(NH_4)_2Fe(SO_4)_2{\cdot}6H_2O$, ≥98 wt%), nickel(II) sulfate hexahydrate ($NiSO_4{\cdot}6H_2O$, ≥99 wt%), cobalt(II) sulfate heptahydrate ($CoSO_4{\cdot}6H_2O$, ≥99 wt%), manganese(II) sulfate monohydrate ($MnSO_4{\cdot}H_2O$, ≥99 wt%), D-(+)-Glucose ($C_6H_{12}O_6$, ≥99.5 wt%) were purchased from Sigma - Aldrich. Aqueous ammonia solution (NH_3, ≥30 wt%), sodium hydroxide (NaOH, ≥99 wt%), acetic acid (CH_3COOH, ≥99 wt%), ethanol (C_2H_5OH, ≥96 v/v.%), hydrochloric acid solution (HCl, ≥37 wt%) were purchased from Xilong Company (China). Direct yellow GX (DYG, $C_{30}H_{26}N_4Na_2O_8S_2$), Moderacid red (RS, $C_{20}H_{11}N_2Na_3O_{10}S_3$) were purchased from Binh Minh company (Vietnam).

2. Preparation of Carbon Coated MFe_2O_4 (C@MFe_2O_4, M= Co, Ni Fe) Nanocomposites

Fe_3O_4 nanoparticles were prepared by co-precipitation method. First, 11.89 g of $FeCl_3{\cdot}6H_2O$ and 8.63 g of $(NH_4)_2Fe(SO_4)_2{\cdot}6H_2O$ were dissolved in 200 ml of distilled water. The mixture was then heated to 80 °C and 10% ammonia solution was slowly dropped into above mixture until pH adjusted to 8-9. The black precipitate of Fe_3O_4 appeared. The reaction was kept at 80 °C for 2 h. The mixture then was let cooled to RT and Fe_3O_4 magnetite nanoparticles were collected by using an external magnet and then Fe_3O_4 magnetite nanoparticles were washed by distilled water to pH=7. In preparation of MFe_2O_4 (M=Mn, Co, Ni Fe) nanoparticles, the $CoCl_2{\cdot}6H_2O$ or $NiCl_2{\cdot}6H_2O$ were used instead of the $(NH_4)_2Fe(SO_4)_2{\cdot}6H_2O$ salt for synthesis of $CoFe_2O_4$, $NiFe_2O_4$ or $MnFe_2O_4$, respectively (Table 1). For preparation of C@MFe_2O_4 (M=Mn, Co, Ni Fe), the synthesized MFe_2O_4 nanoparticles were re-dispersed into distilled water, and 5 g of glucose was added to this suspension, which was then stirred at 200 rpm by magnetic stirrer to dissolve glucose. These suspensions were transferred into the autoclave and the hydrothermal processes were carried out at 160 °C for 8 h. Finally, autoclaves were cooled to RT and C@MFe_2O_4 were collected by using an external magnet and then Fe_3O_4 magnetite nanoparticles were washed by distilled water to pH7; then they were dried at 90 °C for 12 h to obtain the C@MFe_2O_4 nanocomposites as black powders.

3. Adsorption of Moderacid Red (RS) and Direct Yellow GX (DYG) Dyes onto C@MFe_2O_4 Nanocomposites

100 mg L^{-1} of RS or DYS dye solutions were prepared by dissolving 0.10 g of corresponding RS or DYG dyes into 1,000 mL distilled water. The stock was diluted to the desired solution. 0.02 g C@MFe_2O_4 nanocomposite as an adsorbent was added into 20 mL solution containing RS or DYG dyes, then the mixtures were agitated at 30 °C and pH 7. A residue solution was obtained each time by using a magnet bar to remove the adsorbent to prevent them getting out of solution. The residue of RS or DYG concentration in the solution was analyzed by spectrophotometric method as described in section 6 below. The adsorption capacity, q (mg g^{-1}) and the percentage removal (H, %) were calculated as the following equations:

$$q = \frac{(C_o - C) \times V}{m}, (mg\ g^{-1}) \quad (1)$$

$$H = \frac{C_o - C_e}{C_o} \times 100\%, (\%) \quad (2)$$

where C_o, C_e are the initial and equilibrium concentration of dye in solution (mg L^{-1}), respectively; C is dye concentration at time t; V is the volume of sample solution using for the experiment (mL) and m is the weight of adsorbent (g). The adsorption of dye onto C@MFe_2O_4 nanocomposites as adsorbents was studied as a function of contact time, mass of adsorbent influent, pH solution and temperature.

4. Characterization and Methods

XRD patterns of MFe_2O_4 nanoparticles and C@MFe_2O_4 nanocomposites were obtained on D8 Advance, Bruker ASX, operated at a CuKα wavelength of 1.542 Å in the range of 2θ=5 to 70° at room temperature. UV-Vis spectra were measured with Agilent 8453 UV-Vis spectrophotometer system. The surface of C@MFe_2O_4 nanocomposites was observed using a Hitachi S4500 scanning electron microscope (FE-SEM). The infrared (IR) spectra were recorded on Nicolet FT-IR Spectrometer model 205 with KBr pellets in the region from 500 cm^{-1} to 4,000 cm^{-1}.

5. Procedure for Measurement of the Zero Point Charge (ZPC)

In general, the ZPC of any adsorbent can be defined as an indi-

Table 1. Compositions of raw materials for preparation of carbon coated MFe_2O_4 (M=/Co, Ni Fe) nanoparticles

Samples	Mass of precursor salts (g)			
	$FeCl_3{\cdot}6H_2O$	$(NH_4)_2Fe(SO_4)_2{\cdot}6H_2O$	$CoCl_2{\cdot}6H_2O$	$NiCl_2{\cdot}6H_2O$
Fe_3O_4	11.89	8.63	0	0
Fe_3O_4/C	11.89	8.63	0	0
$CoFe_2O_4$/C	11.50	0	6.19	0
$NiFe_2O_4$/C	11.55	0	0	5.78

cation of the electrical balance existing between the adsorbent surface and the dye (in this case) present in the solution. To determine the ZPC of Fe_3O_4 nanoparticles and C@Fe_3O_4 nanocomposite, a total of nine different vials with a volume of 10 mL was prepared for each adsorbent and filled with solution comprising 0.02 M KNO_3 salt. After that, the initial pH value (pH_i) of each solution in vials was tuned using HCl and NaOH. As follows, 0.01 g of each adsorbent was poured into the prepared vials and then stirred for 24 h to reach equilibrium. The final pH value (pH_f) was then measured. Finally, the measured difference between the initial (pH_i) and final pH (pH_f) values was depicted as a function of pH_i: $\Delta pH_{(f-i)}$= $pH_f - pH_i$. This is the intersection between the sketched curve and horizontal axis, which is an indication of ZPC [35-37].

6. Determination of Dye Concentration

The RS or DYG dye concentration after adsorption process was determined by spectrophotometric method combining calibration curves. First, stock solutions of RS and DYG were diluted to 50, 25, 12.5, 6.25 and 3.125 mg L^{-1}. Then, these solutions were measured for the UV-Vis spectra. The maximal absorbance at wavelength (λ=524 nm for RS and at λ=392 nm for DYG) was used to generate the calibration curve of absorbance (A) vs. concentration (C) for RS and DYS concentration determination, respectively. The calibration curves for DYG and RS concentration calculations are shown in Fig. S1.

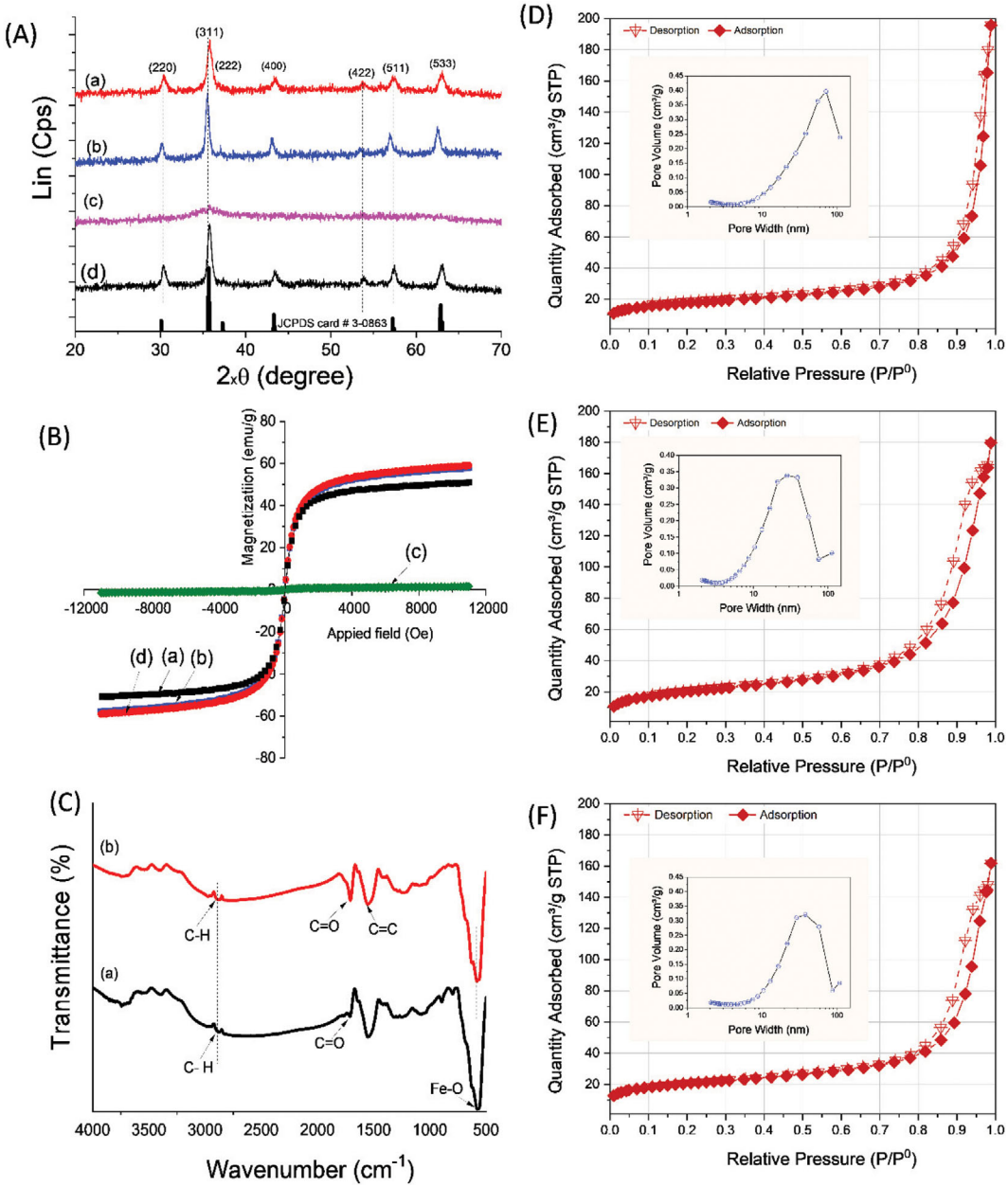

Fig. 1. (A) XRD spectra and (B) VSM of (a) C@Fe_3O_4, (b) C@$CoFe_2O_4$, (c) C@$NiFe_2O_4$ and (d) Fe_3O_4 nanoparticles; (C) FT-IR and (D)-(F) Nitrogen (N_2) adsorption-desorption isotherm of the as-synthesized samples: (D) Fe_3O_4 and (E) C@Fe_3O_4 and (F) C@$CoFe_2O$, nanocomposite, respectively (inserted figures in (D), (E), (F): pore width distribution of the corresponding sample).

Table 2. Surface area, surface area of pore, volume of pores and average pore width of synthesized Fe_3O_4; C@Fe_3O_4 and C@$CoFe_2O_4$

Samples	BET surface area (m^2/g)	BJH surface area of pores(*) (m^2/g)	BJH volume of pores(*) (cm^3/g)	BJH average pore width(*) (nm)
Fe_3O_4	61.47±0.44	37.97÷39.56	0.266÷0.291	26.94÷30.71
Fe_3O_4/C	72.25±0.31	57.09÷62.89	0.25÷0.27	15.97÷18.97
$CoFe_2O_4$/C	71.27±0.63	43.28÷47.85	0.217÷0.237	18.97÷21.87

(*)Calculated from adsorption or desorption process

RESULTS AND DISCUSSION

1. Characterization of Synthesized C@MFe_2O_4 Nanoparticles

The XRD pattern of Fe_3O_4 nanoparticles (Fig. 1(A), curve (d)) and carbon coated MFe_2O_4 (M=Fe, Co) nanocomposites (are denoted: C@MFe_2O_4) ((Fig. 1(A), curve (a), curve (b), respectively) show specific diffraction peaks of Fe_3O_4 which appeared at 2θ=30°, 35°, 57° and 63° corresponding to the reflection of (220), (311), (511) and (440) (JCPDS card # 3-0863), respectively[38]. Exception, the XRD pattern of the C@$NiFe_2O_4$ nanocomposite (Fig. 1(A), curve (c)), above peaks particles did not appear, which implied that $NiFe_2O_4$ was not well crystallized under experimental conditions. Using Debye-Scherrer equation for the (311) peak, it is revealed that the lattice particle size of magnetite particles was 15.35, 12.68 and 20.66 nm in the Fe_3O_4 nanoparticles, C@Fe_3O_4 and C@$CoFe_2O_4$ nanocomposite samples, respectively. EDX spectra of synthesized samples (Fig. S2) confirmed the presence of main elements in each sample, i.e., Fe, O in sample Fe_3O_4; C, Fe, O in sample C@Fe_3O_4, and C, Fe, O, Ni in sample C@$NiFe_2O_4$, and Co, C, Fe, O in sample C@$CoFe_2O_4$, respectively. In the composite sample, the mass of carbon around 8.39-19.35 wt%, and the ratio of Fe/Co and Fe/Ni are nearly 2 : 1, which implies that MFe_2O_4 (with M=Fe, Co, Ni) has stable spinel structure.

The magnetization curves (Fig. 1(B)) of Fe_3O_4 (curve (d)), C@Fe_3O_4 (curve (a)), C@$CoFe_2O_4$ (curve (c)) and C@$NiFe_2O_4$ (curve (b)) show that all samples have super paramagnetic properties with the saturation magnetization (M_s) values of 60, 50 and 58 emu g^{-1} for Fe_3O_4, C@Fe_3O_4 and C@$CoFe_2O_4$, respectively. However, M_s is only of 1.2 emu g^{-1} for C@$NiFe_2O_4$, which is too low for recoverable purpose by using a normal external magnet. Therefore, only Fe_3O_4, C@Fe_3O_4, C@$CoFe_2O_4$ nanocomposites have been used for further applications. It is well known that amorphous carbon is nonmagnetic, so the magnetic behavior of the synthesized C@MFe_2O_4 materials is from magnetite nanoparticle core. The reduction on M_s of C@Fe_3O_4 (50 emu g^{-1}) than that of Fe_3O_4 (M_s=60 emu g^{-1}) can be attributed to the covered Fe_3O_4 nanoparticles by carbon making the saturation magnetization reduced [39].

FTIR spectroscopy (Fig. 1(C)) of Fe_3O_4 and C@Fe_3O_4 nanocomposite shows a broad band occurs in the range of 3,744.3 cm^{-1} corresponding to the stretching mode of free O-H group and physisorbed water. A peak at 2,973.4 cm^{-1} can be assigned to the -C-H stretching and the peaks at 1,714, 1,554, 1,237.53 and 574 cm^{-1} assigned to -C=O, -C=C, -C-O and Fe-O stretching. Especially, on the spectrum of C@Fe_3O_4 sample, there are peaks at 1,317-1,084 cm^{-1} which are assigned to the C-OH stretching on the carbon's surface [40-42], which is good agreement with the previous study [43] and Raman spectra [44,45] (data not shown). The hysteresis loop of the nitrogen adsorption-desorption isotherm for the Fe_3O_4 (Fig. 1(D)) and C@Fe_3O_4 (Fig. 1(E)) and C@$CoFe_2O_4$ (Fig. 1(F)) nanocomposite exhibits type IVa hysteresis loops by IUPAC, which is specific to mesoporous materials with pore width ranging from ~16 to ~31 nm [46]. The BJH pore size distribution of C@Fe_3O_4 sample (Fig. 1(E), insert) shows the main pore diameters are less than 20 nm, which is in high agreement with the shape of the hysteresis loop above (Fig. 1(E)). The BET specific surface area, BJH surface area of pore, BJH volume of pores and BJH average pore width of the synthesized Fe_3O_4, C@Fe_3O_4 and C@$CoFe_2O_4$ samples are summarized in Table 2. SEM images in Fig. 2 show that Fe_3O_4 (Fig. 2(a)-(b)) and C@Fe_3O_4 (Fig. 2(d)-(e)) particles are nearly spherical with a size of 20-30 nm. C@Fe_3O_4 particles have bigger size than that of Fe_3O_4 and agglomeration occurs in C@Fe_3O_4 much less than in Fe_3O_4 sample. TEM images (Fig. 2(c), Fig. 2(f)) show the presence of a thin outer shell structure around spherical Fe_3O_4 particles (Fig. 2(f)). It can be observed that all Fe_3O_4 nanoparticles have been completely covered by a carbon layer with a thickness estimated around 2-3 nm in TEM image. Similar results have been also obtained with C@$CoFe_2O_4$ and C@$NiFe_2O_4$ samples, which clearly demonstrated the successfully synthesis of the carbon coated magnetite nanocomposite C@MFe_2O_4 (M=Fe, Co, Ni) for many applications including adsorption process for heavy metal ion removal, organic dye removal, protein or DNA separation.

2. Evaluation of the Adsorption of RS and DYG onto Nanosorbents

One of the important parameters in the adsorption process is pH; change in pH could form some different ionic species on the adsorbent surface so it affects directly the adsorptive behavior of dyes to adsorbent. The point of zero charge pH_{ZPC} of Fe_3O_4 and C@MFe_2O_4 was evaluated and obtained, showing that they have same the pH_{ZPC}~5.0 (Fig. S3), which implies that the surface of Fe_3O_4 and C@MFe_2O_4 is neutral (non-charge) at pH 5. At pH<5 (pH<pH_{ZPC}), surface of these adsorbents exhibits cationic behavior (positive charge); meanwhile, at pH>5 (pH>pH_{ZPC}) the surface of adsorbent becomes negatively charged. Fig. 3(A) indicates that RS (structure (i)) and DYG (structure (ii)) are almost anionic dyes, so at low pH the electrostatic interaction is increasing between anionic RS and DYG dyes with cationic surface of Fe_3O_4 and C@MFe_2O_4; therefore the obtained adsorption efficiency increases. In addition, Fig. 3(A) shows that RS (structure (i)) has three-negative charge tails (-SO_3^- group) and one positive charge (=N-NH-group); meanwhile, DYG (structure ii) has only two negative charge tails (-SO_3^- group), but it has two positive charged (-N=N-group), which reveals that RS can be easily removed via electrostatic interaction

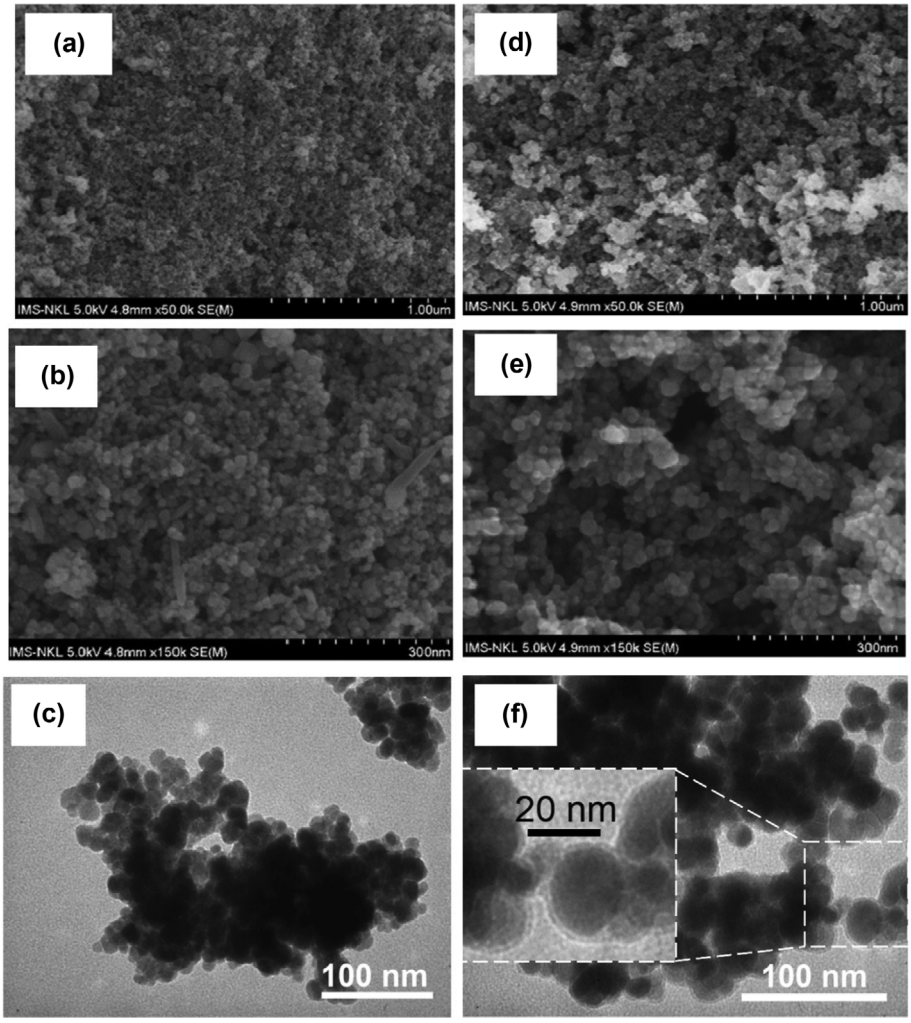

Fig. 2. SEM ((a), (b), (d), (e)) and TEM ((c), (f)) of Fe_3O_4 nanoparticles ((a), (b), (c)) and C@Fe_3O_4 nanocomposites ((d), (e), (f)), respectively.

between anionic tails of dyes with cationic centers on adsorbent surface than that of DYG. This hypothesis has been confirmed by experimental results of the effect of pH on removal efficiency (%) of RS and DYG via adsorption on C@MFe_2O_4 adsorbent in pH range from pH 2 to pH 9 (Fig. 3(B)). The obtained results also disclosed that C@MFe_2O_4 adsorbent has stronger attraction to RS dye molecules (with maximum removal ~100%) than that of DYG (with maximum removal percentage ~40%).

3. Thermal Kinetic Parameters

Results on effect of temperature on adsorption of DYG and RS onto C@Fe_3O_4 adsorbent (Fig. 3(C)) shows that RS has been adsorbed onto C@Fe_3O_4 adsorbent better than DYG at all evaluated temperature; in addition, results also implied that these two adsorption processes were favored at low temperature. The thermodynamic parameters of the adsorption process, such as enthalpy change (ΔH^o), entropy change (ΔS^o) and Gibbs free enthalpy change (ΔG^o) of reaction, were calculated following the second law of thermodynamics, which have been described by following equations (Eq. (3)):

$$\Delta G^o = \Delta H^o - T \times \Delta S^o = -R \times T \times \ln K_D \quad (3)$$

In addition, the equilibrium constant of chemical adsorption process (K_D) can be calculated from experimental data via equation (Eq. (4)):

$$K_D = \frac{q_e}{C_e} \quad (4)$$

Therefore, the relation of K_D with the important thermodynamic parameters of the adsorption process can be established following equation (Eq. (5)):

$$\ln K_D = \frac{-\Delta H^o}{R} \cdot \frac{1}{T} + \frac{\Delta S^o}{R} \quad (5)$$

where R is gas constant (R=8.314 J mol^{-1} K^{-1}); K_D is equilibrium constant of chemical reaction, T is absolute temperature (K). A plot of $\ln K_D$ vs. 1/T following Eq. (5) is shown in Fig. 3(D), wherein, the ΔH^o, ΔS^o values have been calculated from the slope and the intercept of the plot with obtained results given in Table S2. The $\Delta G^o<0$ for RS adsorption process indicates the process is spontaneous for all evaluated temperatures (Table S2). In contrast, $\Delta G^o>0$ for DYG adsorption process reveals that the adsorption of DYG onto C@Fe_3O_4 is non-spontaneous for all evaluated temperatures, and it was more difficult than that of RS. The $\Delta H^o<0$ for DYG

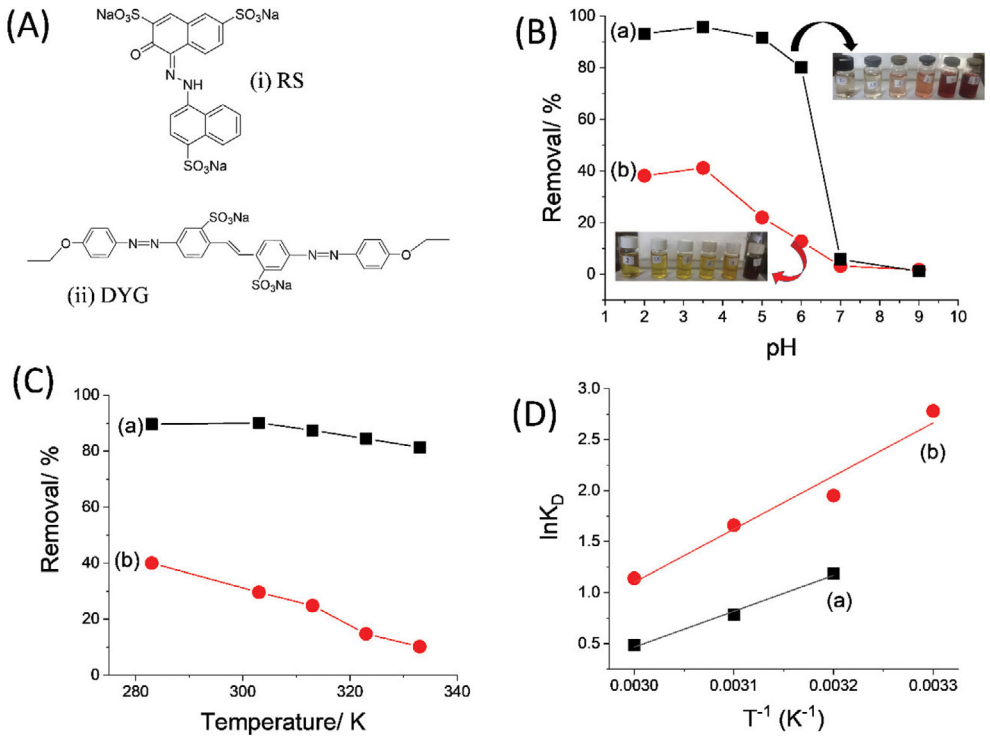

Fig. 3. (A) Molecular structures of (i) RS and (ii) DYG; (B)-(D) Adsorption of (a) RS and (b) DYG, respectively, onto the C@Fe_3O_4 nanocomposite: (B) Effect of pH; (C) Effect of operating temperature on the removal percent (%), respectively. (D) Plot of lnK_D vs. T^{-1} for determining thermal kinetic parameters.

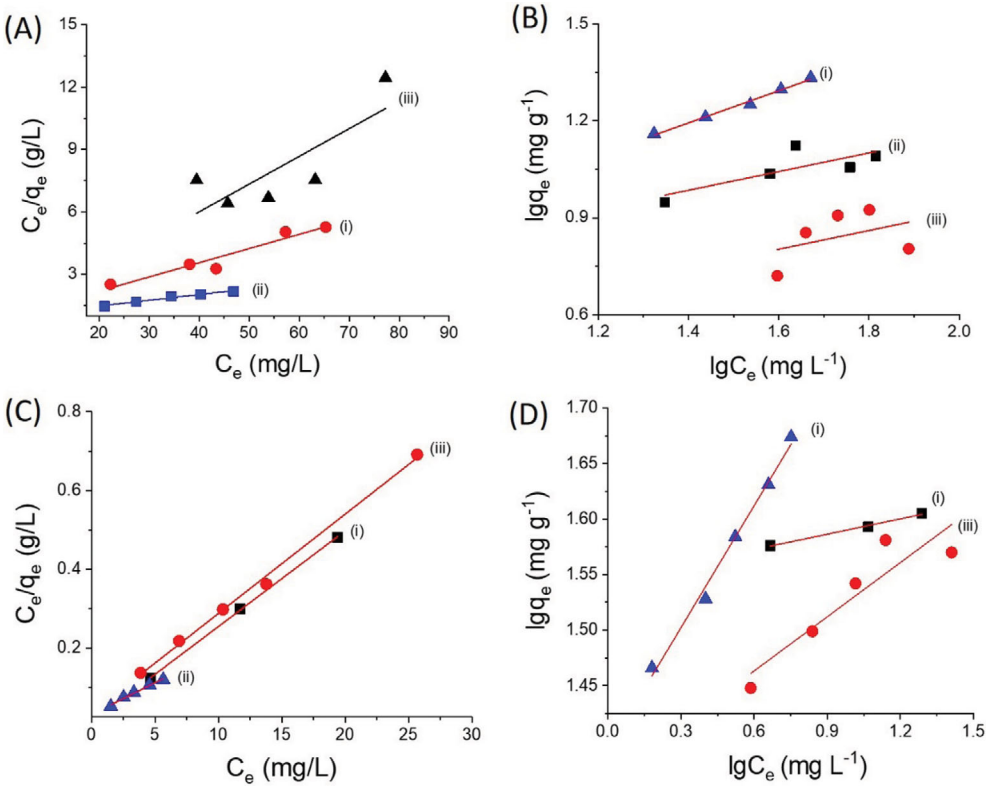

Fig. 4. ((A), (C)) Langmuir and ((b), (d)) Freundlich isotherms for DYG ((A), (B)) and RS ((C), (D)) adsorption onto (i) Fe_3O_4 nanoparticles (black solid square, ■), (ii) Fe_3O_4/C (blue solid upper triangular, ▲) and (iii) $CoFe_2O_4$/C (red solid circle, ●) nanocomposites, respectively.

and RS adsorption process confirms that the adsorption is exothermic and favored by low temperature; and $\Delta S^o<0$ shows the decreasing of the randomness of the adsorbed dye molecules on adsorbent surface.

4. Adsorption Isotherm

To describe the distribution and interactive behavior between the Fe_3O_4 and $C@MFe_2O_4$ adsorbents (as solid state) and organic RS, DYG dyes in aqueous solution (as liquid phase), two adsorption isotherms, Langmuir and Freundlich model, were used. It is well known that the Langmuir model (Eq. (6)) assumes a monolayer adsorption onto the homogeneous surface; there is no transmigration of adsorbate on the surface plane:

$$\frac{C_e}{q_e}=\frac{1}{K_L\cdot q_{max}}+\frac{1}{q_{max}}\cdot C_e \quad (6)$$

In a contrast, the Freundlich model (Eq. (7)) assumes a multilayer adsorption onto the heterogeneous surface:

$$\lg q_e=\lg K_F+\frac{1}{n}\lg C_e \quad (7)$$

where q_{max} (mg g^{-1}) is the maximum adsorption capacity of DYG and RS onto Fe_3O_4, $C@Fe_3O_4$ and $C@CoFe_2O_4$ adsorbents; K_L, K_F are the Langmuir constant and Freundlich constants, respectively; n is a constant. Experimental results following on the Langmuir and Freundlich adsorption isotherms are shown in Fig. 4 and the fitted results for the Langmuir and Freundlich constant are given in Table 3 for DYG dye and Table 4 for RS dye, respectively. For the DYG removal, higher correlation coefficients (R^2) were obtained for Langmuir model than that of Freundlich model (Table 3), which implied that Langmuir model was better fitted than Freundlich. The higher correlation factor (R^2) values suggest that the sorption of DYG onto Fe_3O_4, $C@Fe_3O_4$ and DYG, RS onto $C@CoFe_2O_4$ adsorbents followed monolayer adsorption process, which can be described by Langmuir isotherm, due to the homogeneity of the

Table 3. Isotherm parameters for DYG adsorption

Adsorbent(s)	Isotherm	Equation	R^2	Q_{max} (mg g^{-1})
Fe_3O_4 nanoparticles	Langmuir	$C_e/q_e=(0.819\pm0.517)+(0.068\pm0.011)\cdot C_e$	0.930	14.641
	Freundlich	$\ln q_e=(0.579\pm0.210)+(0.290\pm0.128)\cdot \ln C_e$	0.630	
$C@Fe_3O_4$	Langmuir	$C_e/q_e=(0.917\pm0.009)+(0.028\pm0.003)\cdot C_e$	0.975	36.232
	Freundlich	$\ln q_e=(0.496\pm0.044)+(0.498\pm0.029)\cdot \ln C_e$	0.990	
$C@CoFe_2O_4$	Langmuir	$C_e/q_e=(0.652\pm3.277)+(0.134\pm0.057)\cdot C_e$	0.647	7.485
	Freundlich	$\ln q_e=(0.336\pm0.664)+(0.291\pm0.382)\cdot \ln C_e$	0.162	

Table 4. Isotherm parameters for RS adsorption

Adsorbent(s)	Isotherm	Equation	R^2	Q_{max} (mg g^{-1})
Fe_3O_4 nanoparticles	Langmuir	$C_e/q_e=(0.012\pm0.001)+(0.024\pm0.004)\cdot C_e$	0.999	41.152
	Freundlich	$\ln q_e=(1.545\pm0.003)+(0.046\pm0.003)\cdot \ln C_e$	0.995	
$C@Fe_3O_4$	Langmuir	$C_e/q_e=(0.031\pm0.004)+(0.016\pm0.001)\cdot C_e$	0.988	61.728
	Freundlich	$\ln q_e=(1.393\pm0.011)+(0.366\pm0.019)\cdot \ln C_e$	0.992	
$C@CoFe_2O_4$	Langmuir	$C_e/q_e=(0.036\pm0.012)+(0.025\pm0.001)\cdot C_e$	0.997	39.683
	Freundlich	$\ln q_e=(1.366\pm0.041)+(0.163\pm0.0398)\cdot \ln C_e$	0.848	

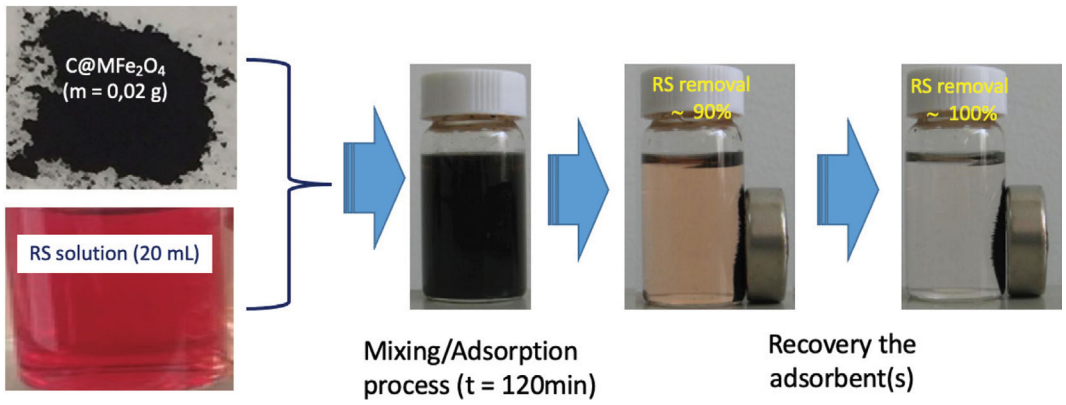

Fig. 5. An illustration of adsorption process for RS removal using $C@Fe_3O_4$ adsorbent.

sorbent surface. In contrast, RS adsorption onto Fe_3O_4 and C@Fe_3O_4 followed Freundlich model (which has the higher R^2), which implies that the adsorption was multilayer sorption process. Distinguishing between the Langmuir and Freundlich model in case of adsorption of RS onto Fe_3O_4, C@Fe_3O_4 and C@$CoFe_2O_4$ adsorbents was not clear because the different of R^2 values were not so big (Table 4), which reveals that the adsorption can be done following both models.

Table 3 and Table 4 also show the maximum monolayer adsorption capacity (q_{max}) for DYG and RS onto various synthesized adsorbents, i.e., Fe_3O_4 nanoparticles, C@Fe_3O_4 and C@$CoFe_2O_4$ nanocomposites, respectively. The highest of q_{max} for RS and DYG was obtained on the C@Fe_3O_4 nanocomposite, which was 36.323 mg g^{-1} for DYG and 61.728 mg g^{-1} for RS, respectively. Notice that these q_{max} were obtained with % removal of 92.685 for RS and 39.678 for DYG (Table S3), which implies that all these adsorbents are more suitable for removal of RS than DYG. In addition, these adsorbents can be recovered using an external magnet (Fig. 5) for desorption process, which has been done by immersing used adsorbent into alkaline solution (NaOH 1 M) for 1 h. A regenerated adsorbent can be obtained by drying for reuse with remaining adsorption capacity *ca.* 95% compared to the original adsorbent.

CONCLUSIONS

We report here a simple experimental process of preparation of C@MFe_2O_4 (where M was Fe, Co, Ni) nanocomposite as a core-shell structure, which then was applied as magnetic adsorbent for RS and DYG removal. Synthesized Fe_3O_4 and C@MFe_2O_4 nanocomposites were well characterized by XRD, FT-IR, SEM, TEM, BET and VSM techniques. In our work conditions, only C@Fe_3O_4 and C@$CoFe_2O_4$ had enough magnetic property for recovery by a normal external magnet, in which these magnetic adsorbents have magnetic nanoparticles as core with the size of 20-30 nm and 2-3 nm in thickness of carbon shell obtained. Adsorption almost followed Langmuir isotherm with q_{max} highest onto C@Fe_3O_4 nanocomposite as 61.728 mg g^{-1} for RS and 36.232 mg g^{-1} for DYG. However, all adsorption isotherm data and thermal kinetic parameters have disclosed that RS can be easily adsorbed onto Fe_3O_4 and C@MFe_2O_4 with a spontaneous process and higher adsorption capacity than that of DYG.

ACKNOWLEDGEMENT

This work was financially supported by the Ministry of Education and Training of Vietnam under project code B2020-SPH-02.

SUPPORTING INFORMATION

Additional information as noted in the text. This information is available via the Internet at http://www.springer.com/chemistry/journal/11814.

REFERENCES

1. S. Abedi and F. Nekouei, *E-J. Chem.*, **8**, 1588 (2011).
2. G. Revathi, S. Ramalingam, P. Subramaniam and A. Ganapathi, *E-J. Chem.*, **8**, 1536 (2011).
3. A. E.-A. A. Said, A. A. M. Aly, M. M. A. El-Wahab, S. A. E.-F. Soliman, A. A. A. El-Hafez, V. Helmey and M. N. Goda, *Energy Environ. Eng.*, **1**, 10 (2013).
4. N. T.-T. Hoang, A. T.-K. Tran, M.-H. Hoang, T. T. H. Nguyen and X.-T. Bui, *Environ. Technol. Innov.*, **21**, 101255 (2020).
5. V. L. Silva, G. Dilarri, C. R. Mendes, R. B. Lovaglio, A. R. Gonçalves, R. N. Montagnolli and J. Contiero, *J. Mol. Liq.*, **321**, 114753 (2021).
6. H. V. Tran, L. T. Hoang and C. D. Huynh, *Chem. Phys.*, **535**, 110793 (2020).
7. H. V. Tran, T. L. Tran, T. D. Le, T. D. Le, H. M. T. Nguyen and L. T. Dang, *Mater. Res. Express*, **6**, 025018 (2018).
8. H. V. Tran, L. T. Bui, T. T. Dinh, D. H. Le, C. D. Huynh and A. X. Trinh, *Mater. Res. Express*, **4**, 035701 (2017).
9. P. P. Hankare, R. P. Patil, A. V. Jadhav, K. M. Garadkar and R. Sasikala, *Appl. Catal. B: Environ.*, **107**, 333 (2011).
10. M. C. Ceballos-Chuc, C. M. Ramos-Castillo, J. J. Alvarado-Gil, G. Oskam and G. Rodríguez-Gattorno, *J. Phys. Chem. C*, **122**, 19921 (2018).
11. Z. A. Al Othman, M. A. Habila, R. Ali, A. A. Ghafar and M. S. El-din Hassouna, *Arabian J. Chem.*, **7**, 1148 (2014).
12. A. Kumar and H. M. Jena, *J. Clean. Prod.*, **137**, 1246 (2016).
13. E. I. El-Shafey, S. N. F. Ali, S. Al-Busafi and H. A. J. Al-Lawati, *J. Environ. Chem. Eng.*, **4**, 2713 (2016).
14. C. A. P. Almeida, N. A. Debacher, A. J. Downs, L. Cottet and C. A. D. Mello, *J. Colloid Interface Sci.*, **332**, 46 (2009).
15. L. Wang, J. Zhang and A. Wang, *Colloids Surf. A: Physicochem. Eng. Asp.*, **322**, 47 (2008).
16. D. Dutta, D. Thakur and D. Bahadur, *Chem. Eng. J.*, **281**, 482 (2015).
17. H. Mittal, A. Maity and S. S. Ray, *Chem. Eng. J.*, **279**, 166 (2015).
18. G. M. K. Tolba, A. M. Bastaweesy, E. A. Ashour, W. Abdelmoez, K. A. Khalil and N. A. M. Barakat, *Arabian J. Chem.*, **9**, 287 (2016).
19. D. M. EL-Mekkawi, F. A. Ibrahim and M. M. Selim, *J. Environ. Chem. Eng.*, **4**, 1417 (2016).
20. T. S. Jamil, H. H. A. Ghafar, H. S. Ibrahim and I. H. A. El-Maksoud, *Solid State Sci.*, **13**, 1844 (2011).
21. A. K. Hammed, N. Dewayanto, D. Du, M. H. A. Rahim and M. R. Nordin, *J. Environ. Chem. Eng.*, **4**, 2607 (2016).
22. Z. Shen, X. Fan, D. Hou, F. Jin, D. O'Connor, D. C. W. Tsang, Y. S. Ok and D. S. Alessi, *Chemosphere*, **233**, 149 (2019).
23. S. S. Yang, Y. Chen, Y. Zhang, H. M. Zhou, X. Y. Ji, L. He, D. F. Xing, N. Q. Ren, S. H. Ho and W. M. Wu, *Environ. Pollut.*, **252**, 1142 (2019).
24. N. Amin, A. Hussain, S. Alamzeb and S. Begum, *Food Chem.*, **136** 1515 (2013).
25. H. Treviño-Cordero, L. G. Juárez-Aguilar, D. I. Mendoza-Castillo, V. Hernández-Montoya, A. Bonilla-Petriciolet and M. A. Montes-Morán, *Ind. Crops Products*, **42**, 315 (2013).
26. H. Kominko, K. Gorazda and Z. Wzorek, *J. Environ. Manage.*, **248** 109283 (2019).
27. Z. M. Xu, Z. Wang, Q. Gao, L.-L. Wang, L.-L. Chen, Q.-G. Li, J.-J. Jiang, H.-J. Ye, D.-S. Wang and P. Yang, *J. Environ. Manage.*, **244** 453 (2019).
28. A. Saeed, M. Iqbal and M. W. Akhtar, *J. Hazard. Mater.*, **117**, 65 (2005).

29. K. Page, M. J. Harbottle, P. J. Cleall and T. R. Hutchings, *Sci. Total Environ.*, **487**, 260 (2014).
30. N. Gupta, A. K. Kushwaha and M. C. Chattopadhyaya, *Arabian J. Chem.*, **9**, S707 (2016).
31. W. Hassan, U. Farooq, M. Ahmad, M. Athar and M. A. Khan, *Arabian J. Chem.*, **10**, S1512 (2017).
32. A. J. B. Leite, E. C. Lima, G. S. dos Reis, P. S. Thue, C. Saucier, F. S. Rodembusch, S. L. P. Dias, C. S. Umpierres and G. L. Dotto, *J. Environ. Chem. Eng.*, **5**, 4307 (2017).
33. R. R. Schio, B. C. da Rosa, J. O. Gonçalves, L. A. A. Pinto, E. S. Mallmann and G. L. Dotto, *Int. J. Biol. Macromol.*, **121**, 373 (2019).
34. M. Atrous, L. Sellaoui, M. Bouzid, E. C. Lima, P. S. Thue, A. Bonilla-Petriciolet and A. B. Lamine, *J. Mol. Liq.*, **294**, 111610 (2019).
35. M. Kosmulski, *J. Colloid Interface Sci.*, **275**, 214 (2004).
36. M. Kosmulski, *J. Colloid Interface Sci.*, **298**, 730 (2006).
37. A. Ebrahimian Pirbazari, E. Saberikhah and S. S. H. Kozani, *Water Resour. Ind.*, **7-8**, 23 (2014).
38. L. Wang, J. Li, Y. Wang, L. Zhao and Q. Jiang, *Chem. Eng. J.*, **181-182**, 72 (2012).
39. A. Millan, A. Urtizberea, N. J. O. Silva, F. Palacio, V. S. Amaral, E. Snoeck and V. Serin, *J. Magn. Magn. Mater.*, **312**, L5 (2007).
40. M. Stoia, C. Păcurariu, R. Istratie and D. Nižňanský, *J. Therm. Anal. Calorim.*, **121**, 989 (2015).
41. X. Bao, Z. Qiang, J.-H. Chang, W. Ben and J. Qu, *J. Environ. Sci.*, **26**, 962 (2014).
42. W. Zhang, L. Y. Zhang, X. J. Zhao and Z. Zhou, *J. Mol. Liq.*, **222**, 995 (2016).
43. G. Z. Kyzas, E. A. Deliyanni and K. A. Matis, *J. Chem. Technol. Biotechnol.*, **89**, 196 (2014).
44. L. Slavov, M. V. Abrashev, T. Merodiiska, C. Gelev, R. E. Vandenberghe, I. Markova-Deneva and I. Nedkov, *J. Magn. Magn. Mater.*, **322**, 1904 (2010).
45. P. C. Panta and C. P. Bergmann, *J. Material. Sci. Eng.*, **5**, 1 (2015).
46. F. Sotomayor, K. A. Cychosz and M. Thommes, *Accounts Mater. Surf. Res.*, **3**, 34 (2018).